Met O (APR) Turbulence and Diffusion Note No. 218

Near-Source Turbulence Parametrization in the Name Model

by

W.L. Physick and R.H. Maryon

14th March 1995

Met O (APR) (Atmospheric Processes Research)
Meteorological Office
London Road
Bracknell
Berkshire, RG12 2SZ

Note:

Near-source turbulence parametrization in the NAME model

by W.L. Physick* and R.H. Maryon#

* Division of Atmospheric Research, CSIRO, Victoria, Australia.
# UK Meteorological Office, MetO(APR).

ABSTRACT

The mesoscale version of the long-range dispersion model NAME uses various forms of the Langevin equation to predict turbulent velocities in the atmospheric boundary layer. These equations, presented in Chapter 2, can be different for horizontal and vertical motion and for stable, neutral and unstable conditions. In Chapter 3, several parametrizations of the vertical variance σ_w and Lagrangian timescale under convectively unstable conditions are evaluated against the Willis and Deardorff (1976, 1978, 1981) laboratory measurements of plume dispersion. The sensitivity of the results to values of the skewness and the universal constant C_0, as well as to the boundary condition at the top of the mixed layer, is also investigated. A scheme which combines a skewed inhomogeneous σ_w profile near the source with a Gaussian homogenous profile further downstream is chosen and presented in Chapter 4. Turbulence profiles for stable and neutral conditions are also specified in this Chapter.

1. INTRODUCTION

The existing long-range versions of NAME deal with sub-grid turbulent diffusion by means of a simple perturbation of particle position in the horizontal and a random reassignment in the vertical in the atmospheric boundary later. This last is because the boundary layer is regarded as well mixed from the outset. More sophisticated random force techniques would prove excessively expensive for a long-range model - the timestep would have to be made very small and the parametrization much more complicated: the ratio of cost to benefit would be unfavourable. The same argument does not apply to the mesoscale problem, where it is essential to pay more attention to the turbulent structure of the boundary layer - especially close to the source. Turbulence must be parametrized in a more detailed manner so that the statistics of the particle perturbation velocities reflect those of the turbulence. In order to achieve this, the velocities are predicted by a form of the Langevin equation which is valid for non-stationary, non-Gaussian and inhomogeneous turbulence.

Through laboratory experiments (Willis and Deardorff, 1976, 1978 and 1981), numerical experiments (Lamb, 1978, Luhar and Britter, 1989) and field experiments (Briggs, 1993a,b), we now understand qualitatively and quantitatively a number of important features of near-source dispersion in a convective boundary layer. These include the descent of the mean plume centreline from an elevated source to a near-source maximum ground-level concentration followed by a rising of the plume before eventually becoming

well-mixed throughout the boundary-layer depth further downwind. It is essential that a mesoscale dispersion model be able to reproduce this behaviour. In this note we evaluate various parametrizations for convective turbulence, including homogeneous and non-homogenous, and Gaussian and non-Gaussian (skewed). As well as testing different values for skewness, we examine a profile in which the skewness itself is inhomogeneous. The influence of the universal constant C_0 in the Langevin equation is also investigated. It is shown that the convective turbulence profile chosen for the mesoscale NAME model is able to reproduce the important features of near- (and far-) source dispersion. Parametrizations for neutral and stable conditions are also presented.

The procedure presented in this Note has been developed to operate over the first 24 hours (or whatever period is selected) following the release of a particle; reversion can then be made to the simpler and cheaper techniques.

2. FORMULATION OF THE MODEL EQUATIONS

Each particle is advected and perturbed according to

$$x(t+\Delta t) = x(t) + \left[u(t) + u'(t)\right]\Delta t$$
$$y(t+\Delta t) = y(t) + \left[v(t) + v'(t)\right]\Delta t$$
$$\eta(t+\Delta t) = \eta(t) + \left[\dot{\eta}(t) + \dot{\eta}'(t)\right]\Delta t$$

where x, y, η are the particle coordinates, $u, v, \dot{\eta}$ the resolved particle velocities which are taken directly from the Unified Model (UM) fieldsfiles, and $u', v', \dot{\eta}'$ the subgrid velocities; the timestep is Δt. The vertical coordinate of UM and NAME, η is defined

$$\eta = \frac{p}{p_*} + A\left(1 - \frac{p_0}{p_*}\right)$$

where p is pressure, p_* surface pressure and p_0 a reference pressure taken as 1000 hPa. η ranges from 1 at the surface to 0 at the 'top' of the atmosphere; A is a function of height chosen so that the coordinate system follows the terrain close to the surface, where $A = 0$, but follows straightforward pressure levels in the stratosphere (where $A = \eta$), with a graduation between.

The subgrid velocities are obtained from a differential equation, first proposed by Langevin in 1908 as a model for Brownian motion. Although a general form of the Langevin equation exists which is valid for non-stationary, non-Gaussian (skewed) and inhomogeneous turbulence (Thomson, 1987), simpler forms of this equation can be applied when the turbulence is assumed to be Gaussian or homogeneous. Skewed can be thought of as meaning that the probability that a sampled velocity will be positive is not the same as that it will be a negative one; in Gaussian turbulence the probabilities are equal. An example of the former is convective turbulence, where downdrafts occupy a greater area than updrafts. By inhomogeneous, we mean varying in space. In this Chapter we present the

different forms of the Langevin equation used in the model according to the type of turbulence being parametrized.

2.1 Stable conditions

We can assume that the turbulence under stable conditions is Gaussian.

2.1.1 Horizontal motion

Assuming that the turbulent eddy motions are uncorrelated among the components the fresh impulse in the x-direction is obtained from the stochastic differential equation (Langevin)

$$du' = a\,dt + b\,d\xi \ , \tag{1}$$

the terms on the RHS representing 'memory' of earlier eddy motion and an innovation respectively. Assuming that the turbulence is Gaussian and homogeneous, we can choose a (the drift or memory coefficient) and b (the diffusion or random coefficient) as follows (see for example Physick and Hurley, 1995):

$$a = -\frac{u'}{\tau_u} \tag{2}$$

$$b = \left(2\frac{\sigma_u^2}{\tau_u}\right)^{0.5} \tag{3}$$

where τ_u is the Lagrangian timescale for the u-component of the turbulence and σ_u^2 is the horizontal velocity variance. The $d\xi$ are increments of a random process; they are here taken as Gaussian with mean zero and variance dt. Thus from (1) - (3) the velocity perturbation can be expressed

$$u'(t+\Delta t) = u'(t)\left(1-\frac{\Delta t}{\tau_u}\right) + \left(\frac{2\sigma_u^2 \Delta t}{\tau_u}\right)^{1/2} r_t \tag{4}$$

$$v'(t+\Delta t) = v'(t)\left(1-\frac{\Delta t}{\tau_u}\right) + \left(\frac{2\sigma_v^2 \Delta t}{\tau_u}\right)^{1/2} r_t \tag{5}$$

where r_t is a random Gaussian variable of zero mean, unit variance.

2.1.2 Vertical motion

Although the above formulation is adequate for the u and v components, where changes in the horizontal are small, the position is more complicated in the vertical as the turbulence is not constant with height, and simply to use $\sigma_{i\eta}(\eta)$ in this type of equation leads to particles tending to collect at levels of small $\sigma_{i\eta}$. To avoid this we must appeal to the Fokker-Planck equation, as discussed in Thomson (1987). By applying the 'well-mixed' condition the Fokker-Planck equation can be used to obtain a modified coefficient a, which accounts for advection across the gradients of $\sigma_{i\eta}$. This takes the form of additional drift terms.

For these conditions (Gaussian inhomogeneous turbulence), it is sufficient to apply the formulation of Wilson et al. (1983) as adjusted by Thomson (1984); skewed turbulence in unstable conditions requires a more complex scheme (see next section).

The Wilson/Thomson model uses a standardized variable $\alpha = \dot{\eta}' / \sigma_{\dot{\eta}}$, and may be expressed as a sequence of operations

$$d\alpha = -\frac{\alpha}{\tau_{\dot{\eta}}}dt + \left(\frac{2}{\tau_{\dot{\eta}}}\right)^{1/2} d\xi + \frac{1}{\rho_\eta}\frac{\partial}{\partial\eta}\left(\sigma_{\dot{\eta}}\rho_\eta\right)dt$$

$$\dot{\eta}' = \alpha\sigma_{\dot{\eta}}$$

$$d\eta = \dot{\eta}\,dt + \dot{\eta}'dt$$

where ρ_η is a density function of air (or equivalently well-mixed pollutant) measured in the x, y, η coordinate system. The system is easily shown to be equivalent to (4,), (5) but with additional drift terms. As ρ_η is constant in η coordinates (in the lower part of the troposphere - we are not concerned with high levels), the 3rd term on the RHS of the top equation simplifies to $\partial\sigma_{\dot{\eta}} / \partial\eta.dt$. Now $\partial\sigma_{\dot{\eta}} / \partial\eta = -1/\rho.\partial(\rho\sigma_w)/\partial z$ is close to the 'known' input profile which is expressed in standard vertical coordinates, $-\partial\sigma_w / \partial z$. Accordingly the system for the vertical perturbation may be expressed.

$$\alpha(t) = \alpha(t-\Delta t)\left(1-\frac{\Delta t}{\tau_{\dot{\eta}}}\right) + \left(\frac{2\Delta t}{\tau_{\dot{\eta}}}\right)^{1/2} r_t - \frac{\partial\sigma_w}{\partial z}\Delta t \qquad (6)$$

$$\dot{\eta}' = \alpha(t)\sigma_{\dot{\eta}} \qquad (7)$$

$$\eta(t+\Delta t) = \eta(t) + \left[\dot{\eta}(t) + \dot{\eta}'(t)\right]\Delta t \qquad (8)$$

Apart from the presence of $\sigma_{\dot{\eta}}$ in (7), this is now a viable system. Consideration of $\dot{\eta}'$ in the general coordinate system $\eta(x,y,z,t)$ shows that

$$\sigma_{\dot{\eta}} \cong \sigma_w \left|\frac{\partial\eta}{\partial z}\right|$$

ignoring terms with horizontal gradients of η; this is readily rearranged to

$$\sigma_{\dot{\eta}} \cong \frac{g\eta}{RT}\sigma_w \qquad (9)$$

where R is the gas constant for dry air, T is temperature and g the acceleration due to gravity. The conditioned particle motion in stable conditions then consists of equations (4) to (9). Note that despite appearances this is essentially the z-coordinate model

$$\begin{aligned}
\alpha(t) &= \alpha(t-\Delta t)\left(1-\frac{\Delta t}{\tau_w}\right)+\left(\frac{2\Delta t}{\tau_w}\right)^{1/2} r_t+\frac{d\sigma_w}{dz}\Delta t \\
w' &= \alpha(t)\sigma_w \\
\dot{\eta}' &= -\frac{g\eta}{RT}w' \\
\eta(t+\Delta t) &= \eta(t)+\left[\dot{\eta}(t)+\dot{\eta}'(t)\right]\Delta t
\end{aligned} \qquad (10)$$

(where α now denotes w'/σ_w) under the transformation (10). With the $\partial\sigma_{\dot{\eta}}/\partial\eta$ approximation the potential advantages of the η - coordinate system (i.e., $\rho_\eta = const$) are lost.

At the upper and lower boundaries of the mixed layer, the reflected velocity of a particle is equal and opposite to the incident velocity (i.e. perfect reflection is applied). New upper boundary conditions to be applied in the NAME model are detailed in 4.3.

2.2 Neutral and unstable conditions

2.2.1 Horizontal motion

In the horizontal direction, Gaussian homogeneous turbulence is assumed and the same equations are used as for stable conditions (Eqs.(1)-(5)). The formulations for $\sigma_{u,v}$ and $\tau_{u,v}$ are of course different (see Chapter 4).

2.2.2 Vertical motion

The turbulence profile in the convectively unstable boundary layer is inhomogeneous, as for stable conditions, but it is also assumed to be non-Gaussian (skewed). [As described in section 4.3, options also exist for homogeneous and Gaussian profiles in the NAME model. Vertical motion for the Gaussian option is dealt with as in 2.1.2.] For skew conditions the general form of the Langevin equation (1) is used, but the drift and diffusion coefficients a and b are specified differently. In this section of the model, it is easier to compute w' in a z-coordinate system, rather than $\dot{\eta}'$ in η-coordinates, and then convert back to $\dot{\eta}'$ to step the particle position forward in time. The corresponding equation to (1) is

$$dw' = adt + bd\xi \qquad (11)$$

where $b=(C_0\varepsilon)^{\frac{1}{2}}$, ε is the rate of dissipation of turbulent kinetic energy and C_0 is a universal constant. Uncertainty surrounds the value of C_0, although 2.0 is usually used for unstable conditions. We evaluate several values in Chapter 3. The Lagrangian timescale τ_w can be related to ε by the relation

$$\tau_w = \frac{2\sigma_w^2}{C_0\varepsilon}.$$

As we shall see, a is a function of σ_w and ε, both measurable quantities, rather than τ_w which is only clearly defined when the turbulence is homogeneous and stationary. Note too that, unlike previous versions of the Langevin equation (for example de Baas et al., 1986, Sawford and Guest, 1987), it is not necessary to incorporate the skewness Sk of the convective boundary layer in the diffusion (random) term, which remains Gaussian.

The finite-difference form of Eq.(11) is

$$w'(t+\Delta t) = w'(t) + a\Delta t + (C_0 \varepsilon \Delta t)^{1/2} r_t \,. \tag{12}$$

After computation of w', $\dot{\eta}'$ is calculated from

$$\dot{\eta}' = -\frac{g\eta}{RT} w' \tag{13}$$

and the new particle position found in the (x, y, η) system.

An expression for the function a is obtained by solving the following form of the Fokker-Planck equation (Thomson, 1987),

$$\frac{\partial (aP_E)}{\partial w} = -\frac{\partial P_E}{\partial t} - \frac{\partial (wP_E)}{\partial z} + \frac{1}{2} C_0 \varepsilon \frac{\partial^2 P_E}{\partial w^2} \tag{14}$$

subject to the boundary condition $aP_E \rightarrow 0$ as $|w'| \rightarrow \infty$ (B.L. Sawford, personal communication, 1988). P_E is the probability density function (PDF) made up of two Gaussian functions, one representing the updrafts (+) and the other representing the downdrafts (-) of the convective boundary layer, and written as

$$P_E = pN(m_+, \sigma_+) + (1-p)N(m_-, \sigma_-) \tag{15}$$

with

$$N(m, \sigma) = \sigma^{-1}(2\pi)^{-0.5} \exp\left(-(w'-m)^2 / 2\sigma^2\right). \tag{16}$$

Here p is the probability of a particle being in an updraft, m_+ is the mean velocity in an updraft and σ_+ is the velocity standard deviation in an updraft, and similarly for the downdraft terms. The first three moments of P_E are equated to the first three moments of the vertical velocity distribution ($0, \sigma_w^2$ and S_w^3 respectively, where $S_w^3 = Sk\,\sigma_w^3$) and the resulting equations are solved for the variables p, m_+, *and* m_-, by making the assumption $\sigma = |m|$ for both updrafts and downdrafts (see for example Hudson and Thomson, 1994).

The solutions are:

$$p = 0.5(1 - (Sk^2 / (8 + Sk^2))^{0.5}) \tag{17}$$

$$m_+^2 = 0.5\sigma_w^2 (1-p)/p \tag{18}$$

$$m_- = -m_+ p/(1-p) \tag{19}$$

where $Sk = (S_w/\sigma_w)^3$ is the degree of skewness of the turbulence.

By means of a little calculus, the solution of Eq.(14) can be shown to be (see for example Luhar and Britter, 1989)

$$a = \frac{\phi_+ + \phi_-}{P_E} \tag{20}$$

where

$$\phi_+ = -\frac{1}{2} C_0 \varepsilon p N_+ (w' - m_+)/\sigma_+^2$$

$$+\sigma_+ N_+ \left(\frac{\partial p \sigma_+}{\partial z} - \frac{pw'}{\sigma_+^2} \left(m_+ \frac{\partial \sigma_+}{\partial z} - \sigma_+ \frac{\partial m_+}{\partial z} \right) + \frac{pw'^2}{\sigma_+^2} \frac{\partial \sigma_+}{\partial z} \right)$$

$$-\frac{1}{2} \frac{\partial p m_+}{\partial z} \left(1 + erf\left(\frac{w - m_+}{\sqrt{2}\sigma_+} \right) \right)$$

with the expressions for ϕ_- of the same form, except with p replaced by 1-p and with subscript "+" replaced by "-". Note that the inner bracket in the second term is zero.

The boundary condition used is one of skewed memory reflection, where w' is scaled by the absolute value of the ratio of the mean updraft velocity to the mean downdraft velocity when reflecting at the ground (w' becomes $-w'(1\text{-}p)/p$). The inverse of this ratio is used in an analogous manner at the top of the mixed layer in the experiments of Chapter 3. Thomson and Montgomery (1994) show that the theoretically correct boundary condition is

$$\int_{-\infty}^{w_i'} w' P_E \, dw' = \int_{w_r'}^{\infty} w' P_E \, dw'$$

where w_i' is the incident velocity and w_r' is the reflected velocity. There is negligible difference between results from either formulation in inhomogeneous turbulence where the moments of the turbulence, or the timescales, usually decrease to zero at the boundaries.

Some runs are done in Chapter 3 where the top boundary condition is removed and particles are allowed to move into a stable region of low turbulence above the mixed layer. There appear to be no problems with particle loss or accumulation at the mixed-layer top and it is recommended that no reflection condition be used in NAME at the upper boundary of the mixed layer. Further discussion can be found in Chapters 3 and 4.

2.3 Computational timestep

The first consideration is that a change in the magnitude of σ_w due to the turbulent vertical motion of a particle should be small in comparison to the size of σ_w itself. That is

$$w'\Delta t\left|\frac{d\sigma_w}{dz}\right| \ll \sigma_w$$

so that to an approximation

$$\Delta t \ll \frac{1}{|d\sigma_w / dz|},$$

for practical purposes taken as

$$\Delta t = \frac{0.05}{|d\sigma_w / dz|}$$

The above expression may give very large values near $d\sigma_w/dz = 0$ and is replaced by

$$\Delta t = \frac{0.05(1-\eta_i)}{|\dot{\eta}'|} \qquad (21)$$

if it is smaller. Here, η_i is the boundary layer top, and $(1-\eta_i)$ the boundary layer depth, in η units. An additional requirement is that the timestep be short in comparison with the Lagrangian timescale, so (20), (21) are subject to the additional constraint.

$$\Delta t \le 0.05\tau_w.$$

The Lagrangian timescales for all conditions of stability are subject to a minimum of 20secs, although they may well be smaller close to the surface. This is to avoid very short computational timesteps. Note that each particle can be followed for a number of timesteps, totalling for example 15 minutes, and then the next particle is followed for the same period and so on. Concentrations may be calculated at the end of such a period. The timesteps are clearly variable in length, so that provision must be made to truncate a timestep when the end of a period of integration has been reached.

3. EVALUATION OF TURBULENCE PROFILES FOR UNSTABLE CONDITIONS

Documentation for all stability conditions of the horizontal and vertical components of the turbulence (variance σ^2 and either Lagrangian timescale τ or turbulence dissipation rate ε) employed in NAME, is presented in Chapter 4. However in this Chapter, we evaluate three turbulence formulations appropriate to unstable conditions, before making a choice for use in NAME. Boundary conditions and skewness values are also examined. The three turbulence schemes are tested here against the laboratory results of Willis and Deardorff (1976, 1978, 1981) for plume dispersion in convective conditions. In these experiments,

neutrally-buoyant oil droplets were released at various levels in a convectively mixed layer generated in a water tank and downstream concentrations monitored.

Inhomogeneous profiles of σ_w and τ_w from Hanna (1982), based on the 1973 Minnesota planetary boundary layer experiment, are evaluated first, followed by the σ_w profile of Hibberd and Sawford (1994) (Fig. 1). The small amount of scatter in the convection tank data upon which the latter profile is based reflects the large amount of sampling under tightly-controlled conditions. The τ_w profile is obtained indirectly by specifying the variation of the TKE dissipation rate with height and using the relation $\tau_w = 2\sigma^2_w / C_o \varepsilon$. The third turbulence formulation tested specifies homogeneous profiles of σ_w and τ_w. As can be seen from the timestep-size relation of section 2.3 (Eq. 20), a homogeneous σ_w profile allows a larger timestep to be used.

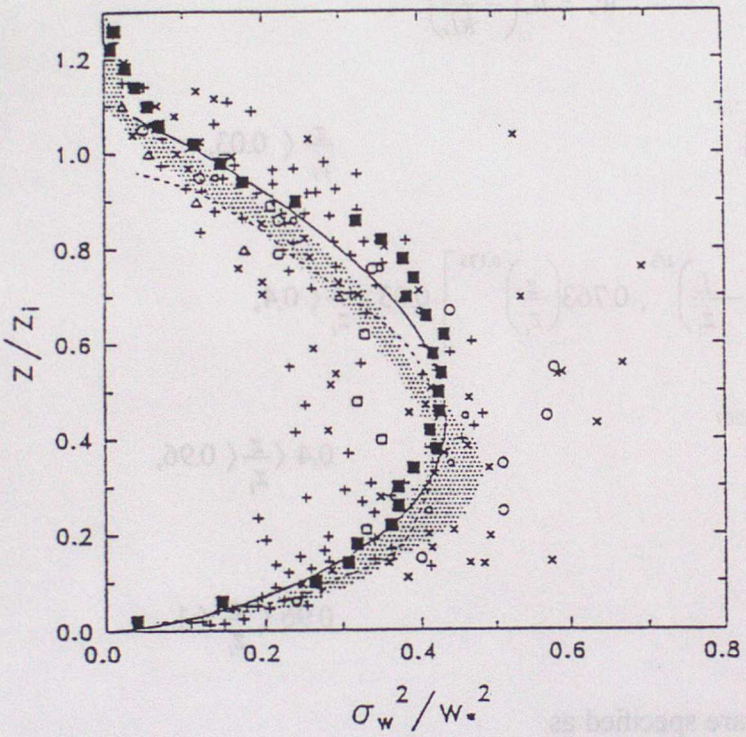

Figure 1. Variance of vertical velocity fluctuations as a function of dimensional height. Hibberd and Sawford, 1994 (■) Willis and Deardorff, 1974, case S1 (O), case S2 (o): Deardorff and Willis, 1985 (□): Caughey and Palmer, 1979 (+): Young, 1988 (X): Kumar and Adrian, 1986 (Δ): Adrian et al., 1986 (----): Range of results from large-eddy simulations of Nieuwstadt et al. 1992 (shaded region ▒): Empirical fit of Equation (22) (—). (From Hibberd and Sawford, 1994).

3.1 Parametrizations

Expressed in z-coordinates (height above the ground), the three parametrizations are

A Hanna (1982)

$\sigma_u = \sigma_v = u_* \left(12 + 0.5 z_i / |L|\right)^{1/3}$ for $\eta \rangle 0.996$ (the surface layer).

$\sigma_u = \sigma_v = \left(0.4 w_*^2\right)^{1/2}$ above (in the mixed layer).

Here L is the Monin-Obhukov length defined as

$$L = -\frac{c_p T_s u_*^3}{kgH},$$

where c_p is the specific heat at constant pressure, k is von Karman's constant, T_s the surface temperature and H the sensible heat flux. L is a quantitative measure of atmospheric stability. z_i is the boundary layer depth, u_* is the friction velocity, and the convective velocity scale, w_*, is defined (for +ve H) as

$$w_* = u_* \left(-\frac{z_i}{kL} \right)^{1/3}.$$

$$\frac{\sigma_w}{w_*} = 0.96\left(3\frac{z}{z_i} - \frac{L}{z_i}\right)^{1/3} \qquad \frac{z}{z_i} < 0.03,$$

$$\frac{\sigma_w}{w_*} = \min\left[0.96\left(3\frac{z}{z_i} - \frac{L}{z_i}\right)^{1/3}, 0.763\left(\frac{z}{z_i}\right)^{0.175}\right] \qquad 0.03 < \frac{z}{z_i} < 0.4,$$

$$\frac{\sigma_w}{w_*} = 0.722\left(1 - \frac{z}{z_i}\right)^{0.207} \qquad 0.4 < \frac{z}{z_i} < 0.96,$$

$$\frac{\sigma_w}{w_*} = 0.37 \qquad 0.96 < \frac{z}{z_i} < 1.$$

The Lagrangian timescales are specified as

$$\tau_u = \tau_v = 0.15\frac{z_i}{\sigma_u}$$

$$\tau_w = \frac{0.1z}{\sigma_w(0.55 + 0.38z/L)} \qquad \text{for} \quad \frac{z}{z_i} < 0.1, \quad -\frac{z}{L} < 1,$$

$$\tau_w = \frac{0.59z}{\sigma_w} \qquad \text{for} \quad \frac{z}{z_i} < 0.1, \quad -\frac{z}{L} \geq 1,$$

$$\tau_w = 0.15\frac{z_i}{\sigma_w}\left[1 - \exp(-5z/z_i)\right] \qquad \text{for} \quad \frac{z}{z_i} \geq 0.1.$$

B Hibberd and Sawford (1994)

$$\sigma_u = \sigma_v = u_*\left(12 + 0.5 z_i / |L|\right)^{1/3} \qquad \text{for} \quad \eta \rangle\ 0.996 \ \text{(the surface layer)}$$

$$\sigma_u = \sigma_v = \left(0.4 w_*^2\right)^{1/2} \qquad \text{above (in the mixed layer)}$$

$$\frac{\sigma_w}{w_*} = \left[1.2\left(\frac{z}{z_i}\right)^{2/3}\left(1 - 0.9\frac{z}{z_i}\right)\right]^{1/2} \qquad (22)$$

$$\varepsilon = \left(1.5 - 1.2\left(\frac{z}{z_i}\right)^{1/3}\right)\frac{w_*^3}{z_i} \qquad \text{(from Luhar and Britter, 1989)}$$

C Hurley and Physick (1993)

$$\sigma_u = \sigma_v = \sigma_w = 0.6 w_*$$

$$\varepsilon = 0.6 w_*^3 / z_i$$

For each formulation, a value of 0.6 is chosen for the skewness at all levels, in agreement with most field data (for example, Wyngaard, 1988, Lemone, 1990). However, the sensitivity to skewness of the results from the Hibberd and Sawford profile is examined later.

3.2 Experimental setup

The Willis and Deardorff experiments examined the time behaviour of an instantaneous line release of passive material (oil droplets) at three heights: z_s=0.067z_i, 0.24z_i and 0.49z_i. There was no mean flow. In our numerical experiments, we release at time t=0, 60000 particles at each of these heights. The positions of these particles, converted to concentrations, are stored at intervals of 0.05T, where T is a non-dimensional time $(w_*/z_i)t$. If we assume Taylor's hypothesis that $t = x/u$, where u denotes windspeed and x downwind distance, then T can also be thought of as the non-dimensional distance $X = xw_*/(uz_i)$. Thus our height-time plots of concentration, and those of Willis and Deardorff, can also be thought of as height-downwind distance plots.

Skewed reflection conditions, as described in section 2.2.2, were used at the top and bottom of the mixed layer. Concentrations were calculated by dividing the mixed layer into 20 boxes of size .05z_i, counting the number of particles in each box, and non-dimensionalizing by the number of particles expected if the profile was well mixed throughout the depth of z_i, i.e.60000 x 0.05. This is equivalent to the non-dimensionalized cross-wind integrated

concentrations measured by Willis and Deardorff. A value of 600 m was used for z_i, 1.5 m s^{-1} for w_*, and -55 m for L.

3.3 Results from the parametrization comparison

Figure 2 shows the dimensionless concentration contours obtained for the three source heights by Willis and Deardorff. The mean centreline of the two elevated plumes descends to the ground, where the maximum ground-level concentration is registered at a distance less than X=1, and then appear to lift off again before finally becoming well mixed throughout the depth of the boundary layer further downwind. The descent of the plume is due to the skewness of the turbulent vertical velocity distribution; slower-moving downdrafts occupy a greater area than the faster updrafts. The plume from the near-surface source ($0.067z_i$) drifts horizontally for a short distance before it too is lifted to the upper reaches of the boundary layer. A well-mixed profile eventually results towards X=4. It should be noted that the mixed layer was growing slowly during these experiments; hence the falling off in concentrations towards the top of the layer. This should not be evident in our numerical experiments where there was no boundary-layer growth and a reflection condition was employed.

Numerical predictions of the plume dispersion using turbulence parametrization **A** (Hanna) are shown in Fig.3 for the three source heights. From a comparison with Fig.2, it is apparent that the plume is being brought to the ground too far from the source, and any subsequent lift-off is almost non-existent. As discussed later, the maximum ground-level concentration (glc) from the two elevated sources is clearly lower than measured in the laboratory experiments. There also appears to be a problem with a deficit of particles near the surface in the well-mixed region further downwind.

Results from parametrization **B** (Hibberd and Sawford) are plotted in Fig.4. The elevated plumes reach the ground only a little further downwind than measured, after which they lift off as observed and become well-mixed throughout the boundary-layer depth further downwind. Simulation of the dispersion from the near-surface source also displays the main observed features. For all sources, there is significantly better agreement between predicted and measured maximum ground level concentrations than for parametrization **A**.

Figure 5 shows the concentrations predicted when the homogeneous parametrization **C** (Hurley and Physick) is used. All the main features are reproduced. The results are surprisingly good; better than parametrization **A**, and barely different than those of **B**. In fact this parametrization is superior in simulating the near vertical or slightly forward-leaning contours near the surface observed after plume lift-off.

Further evaluation of the three schemes can be carried out by examining the predictions of ground level concentration as a function of downwind distance (Fig.6). Also shown are the data points from the laboratory experiments. For the elevated sources, the magnitudes of the predicted maxima are smaller than observed and the locations of these maxima are generally a little further downwind than was observed. For all three sources the predicted plume lift-off (glc less than 1.0) is not as pronounced, as evidenced by the higher concentrations predicted at this time. Parametrization **A** performs poorly for the elevated sources and as suspected previously, does not produce a well-mixed profile far from the

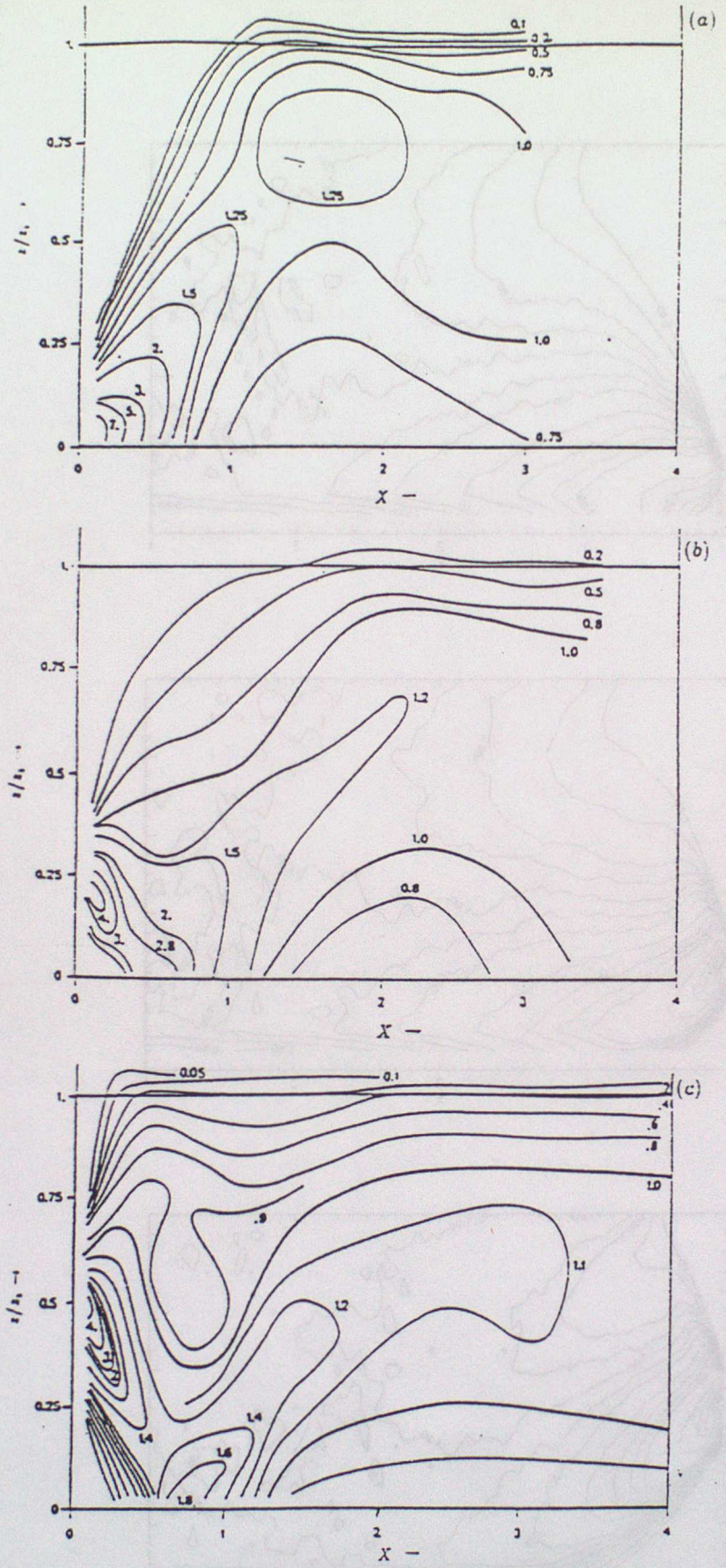

Figure 2. Contours of the non-dimensional cross-wind integrated concentrations obtained by Willis and Deardorff for the three source heights (z_s/z_i): (top) 0.067, (middle) 0.24, and (bottom) 0.49.

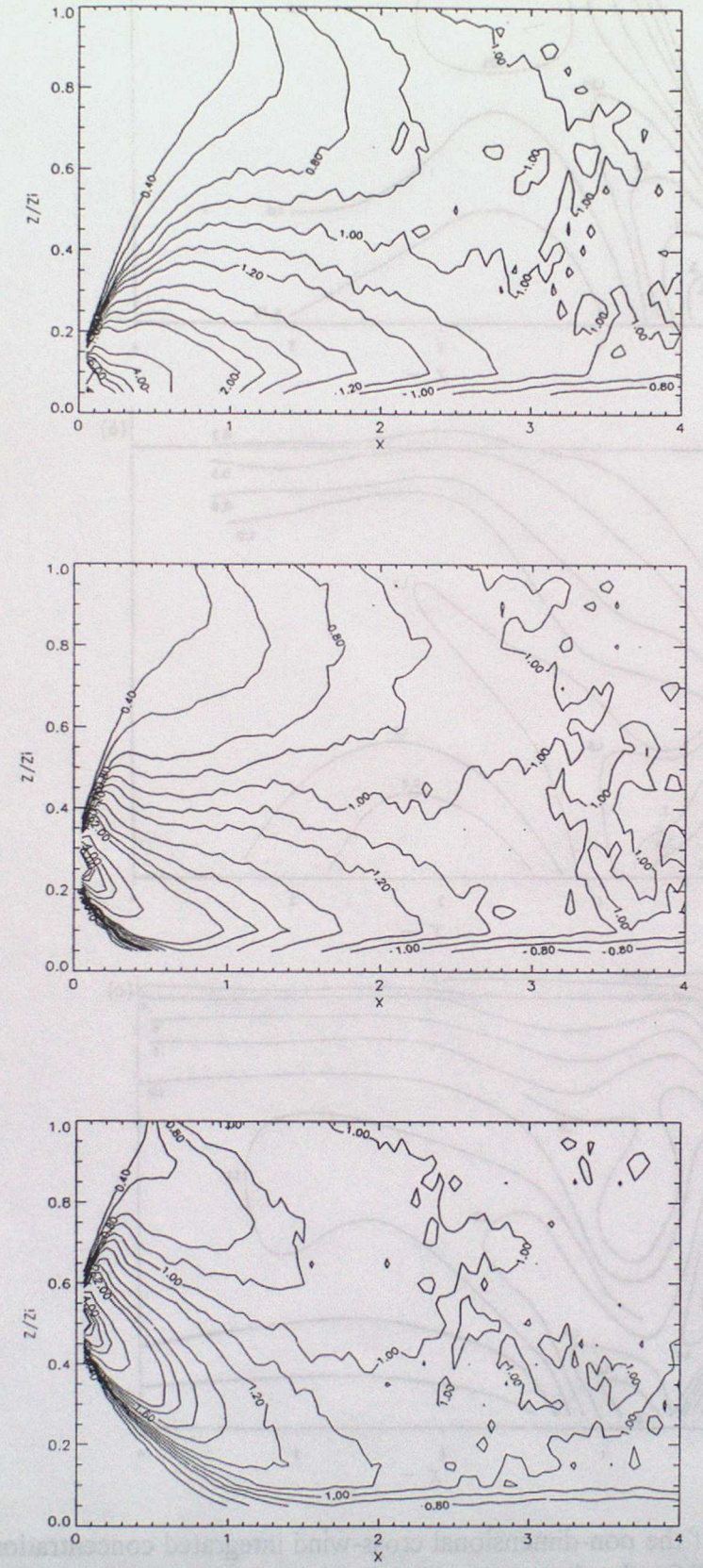

Figure 3. Contours of the non-dimensional cross-wind integrated concentrations predicted by the model using parametrization **A** (Hanna) for the three source heights (z_s/z_i): (top) 0.067, (middle) 0.24, and (bottom) 0.49.

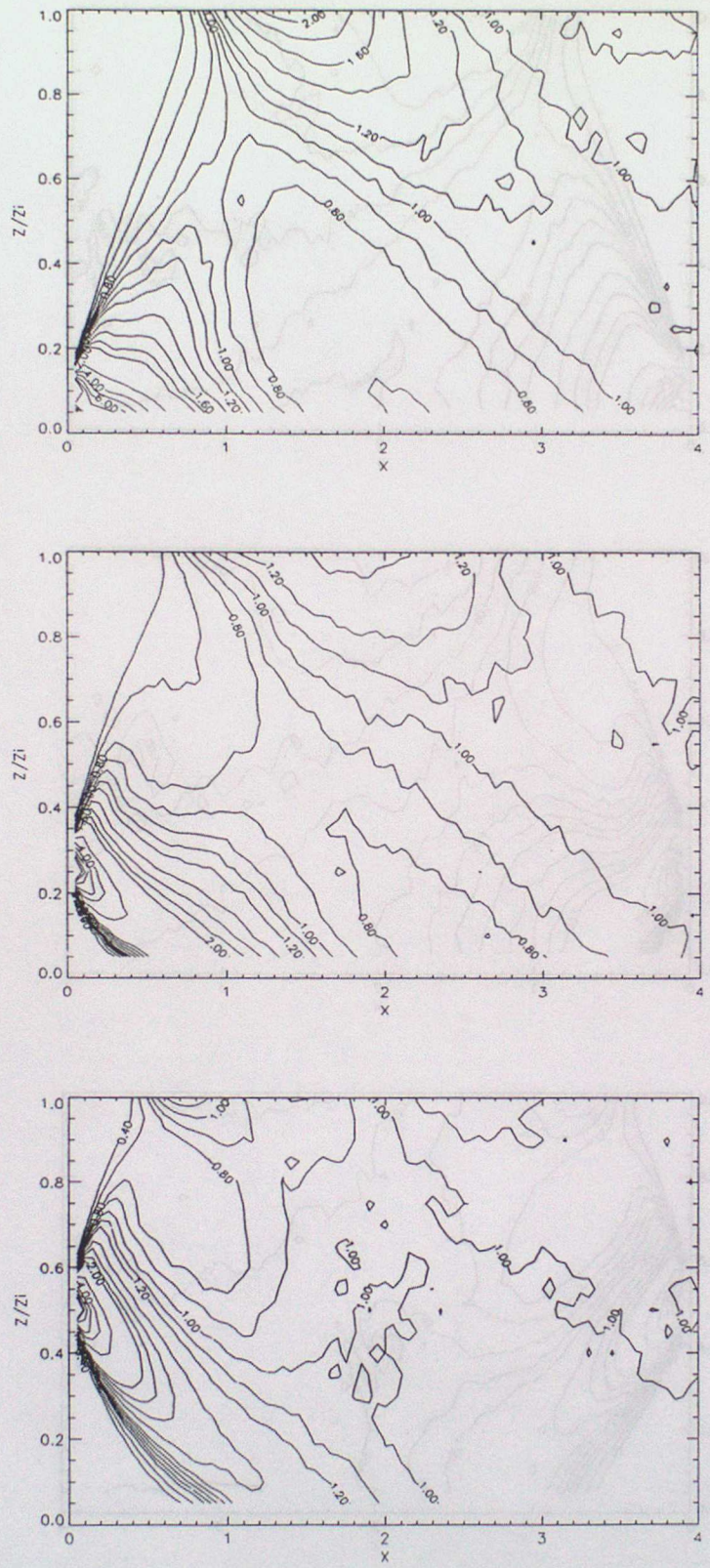

Figure 4. Contours of the non-dimensional cross-wind integrated concentrations predicted by the model using parametrization **B** (Hibberd and Sawford) for the three source heights (z_s/z_i): (top) 0.067, (middle) 0.24, and (bottom) 0.49.

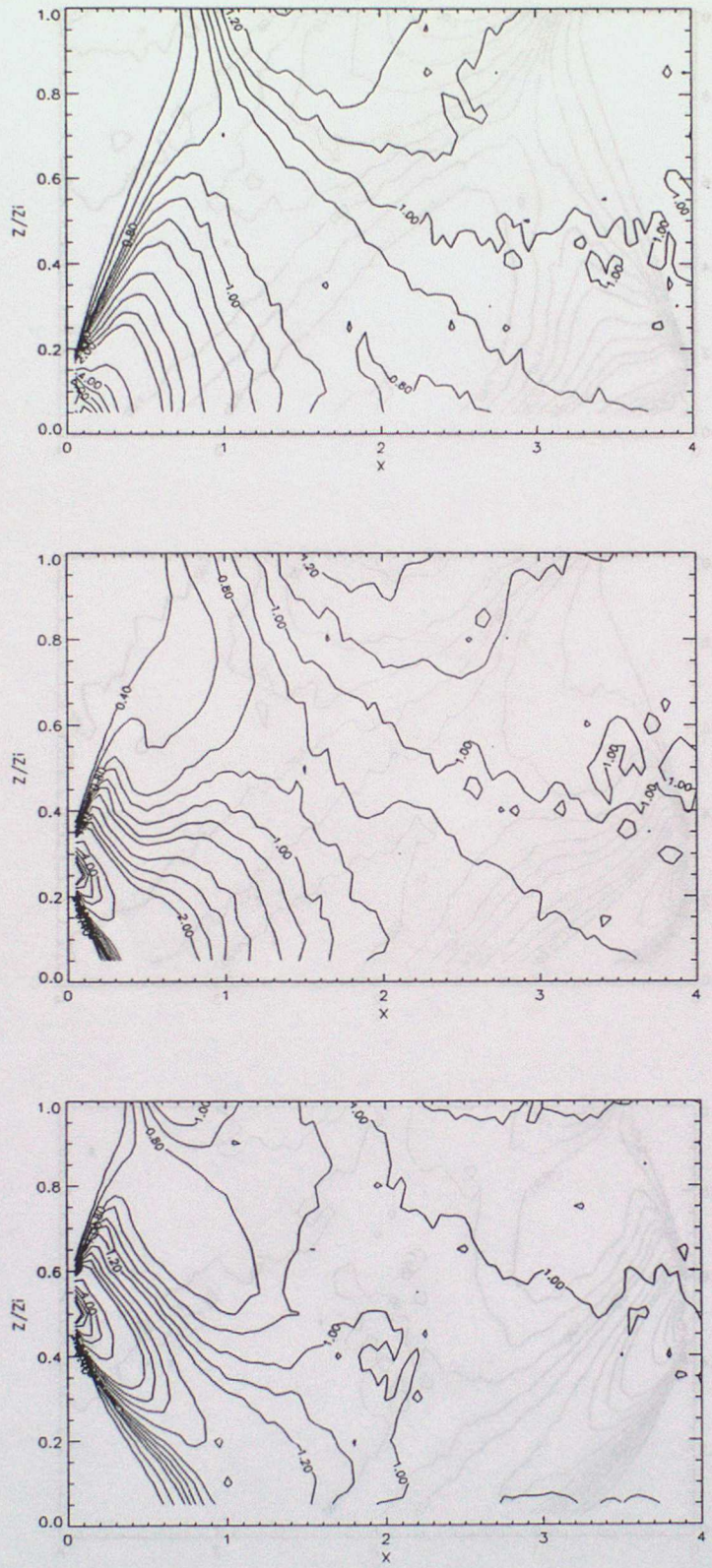

Figure 5. Contours of the non-dimensional cross-wind integrated concentrations predicted by the model using parametrization **C** (Hurley and Physick) for the three source heights (z_s/z_i): (top) 0.067, (middle) 0.24, and (bottom) 0.49.

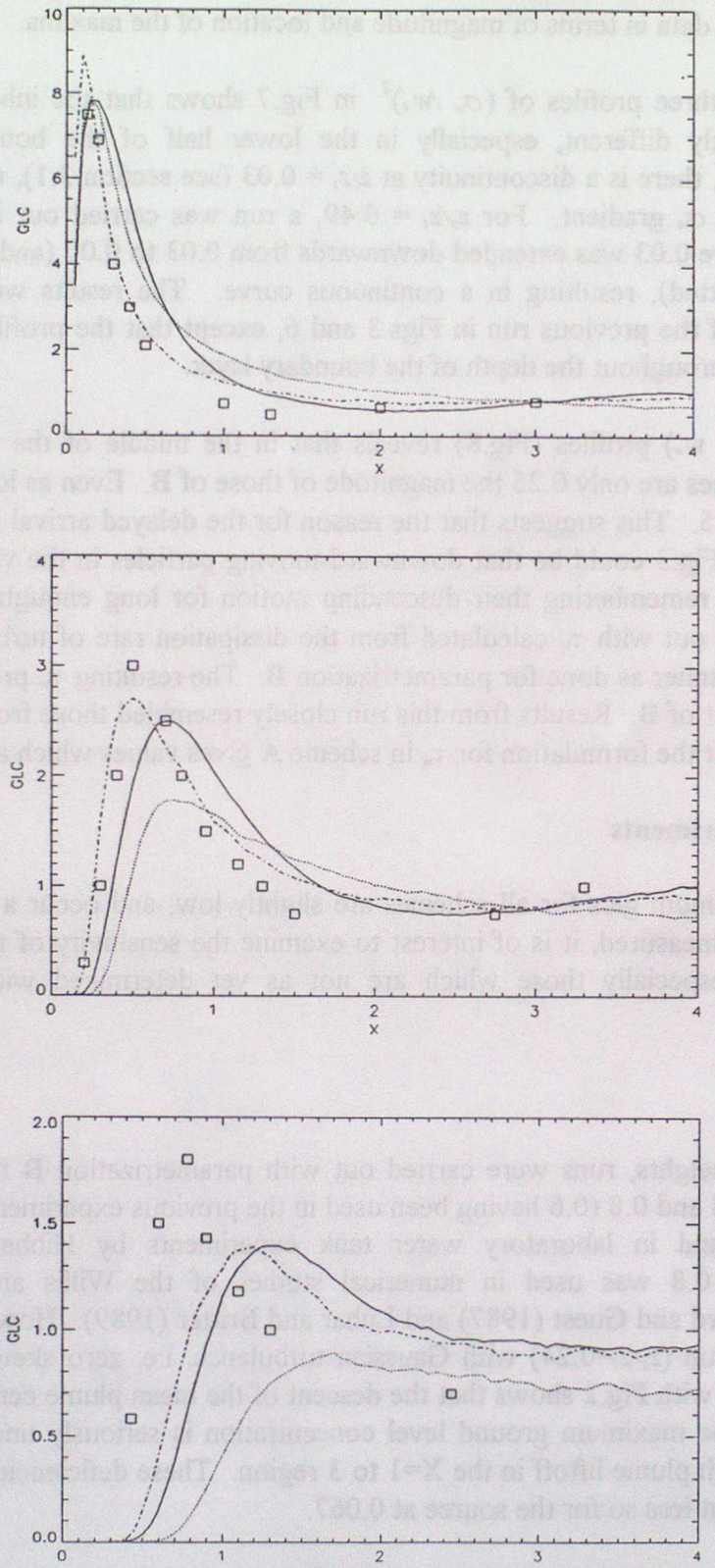

Figure 6. Non-dimensional cross-wind integrated ground-level concentrations as a function of downwind distance, for source heights (z_s/z_i): (a) 0.067, (b) 0.24, and (c) 0.49. Parametrization A (dotted curve), B (solid curve), and C (dot - dash curve). Measurements of Willis and Deardorff (□).

source. There is not a lot to choose between schemes **B** and **C**, although **C** is probably closer to the measured data in terms of magnitude and location of the maxima.

A comparison of the three profiles of $(\sigma_w / w_*)^2$ in Fig.7 shows that the inhomogeneous profiles are not greatly different, especially in the lower half of the boundary layer. However in scheme **A**, there is a discontinuity at $z/z_i = 0.03$ (see section 3.1), resulting in a change of sign of the σ_w gradient. For $z_s/z_i = 0.49$, a run was carried out in which the expression for σ_w above 0.03 was extended downwards from 0.03 to 0.00 (and the surface-layer formulation omitted), resulting in a continuous curve. The results were not very different from those of the previous run in Figs.3 and 6, except that the profile downwind was now well-mixed throughout the depth of the boundary layer.

Examination of $\tau_w/(z_i/ w_*)$ profiles (Fig.8) reveals that in the middle of the mixed layer, parametrization **A** values are only 0.25 the magnitude of those of **B**. Even as low as $0.1z/z_i$, the ratio is still only 0.5. This suggests that the reason for the delayed arrival of the plume at the ground seen in Fig.3 could be that downward-moving particles in the vicinity of the source height are not remembering their descending motion for long enough. A run for scheme **A** was carried out with τ_w calculated from the dissipation rate of turbulent kinetic energy in the same manner as done for parametrization **B**. The resulting τ_w profile was not very different from that of **B**. Results from this run closely resembled those from scheme **B** (Fig.4), confirming that the formulation for τ_w in scheme **A** gives values which are too low.

3.4 Sensitivity experiments

As the predicted maximum glcs for all schemes are slightly low, and occur a little further from the source than measured, it is of interest to examine the sensitivity of the results to various parameters, especially those which are not as yet determined with any great accuracy.

3.4.1 Skewness

For all three source heights, runs were carried out with parametrization **B** for additional skewness values of 0.4 and 0.8 (0.6 having been used in the previous experiments). A value of 0.4 has been found in laboratory water tank experiments by Hibberd (personal communication) and 0.8 was used in numerical studies of the Willis and Deardorff experiments by Sawford and Guest (1987) and Luhar and Britter (1989). However we first show results from a run (z_s/z_i=0.24) with Gaussian turbulence, i.e. zero skewness (Figs.9 and 10). Comparison with Fig.2 shows that the descent of the mean plume centreline is not simulated properly, the maximum ground level concentration is seriously underestimated, and there is not enough plume liftoff in the X=1 to 3 region. These deficiencies are greater for the 0.49 source, but less so for the source at 0.067.

For the non-zero values of skewness, our results show that there are no great differences in the predicted dispersion patterns over the range examined. Comparisons of ground level concentrations can be seen in Fig.11. The trend is for higher skewness values to give higher maximum ground level concentrations, and these are found further from the source than those with lower skewness values. This arises from the fact that in a boundary layer with higher skewness, plume material is more likely to be found in a downdraft than it is with

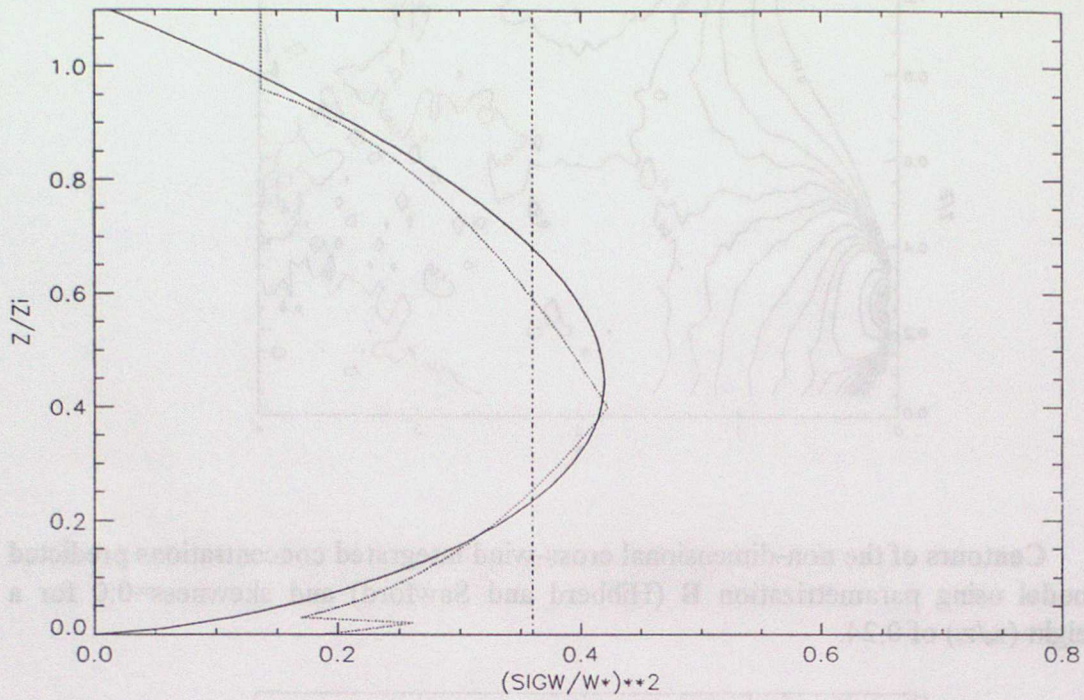

Figure 7. Profiles of $(\sigma_w/w_*)^2$ as a function of non-dimensional height z/z_i, for parametrizations **A** (dotted curve), **B** (solid curve) and **C** (dash - dot curve).

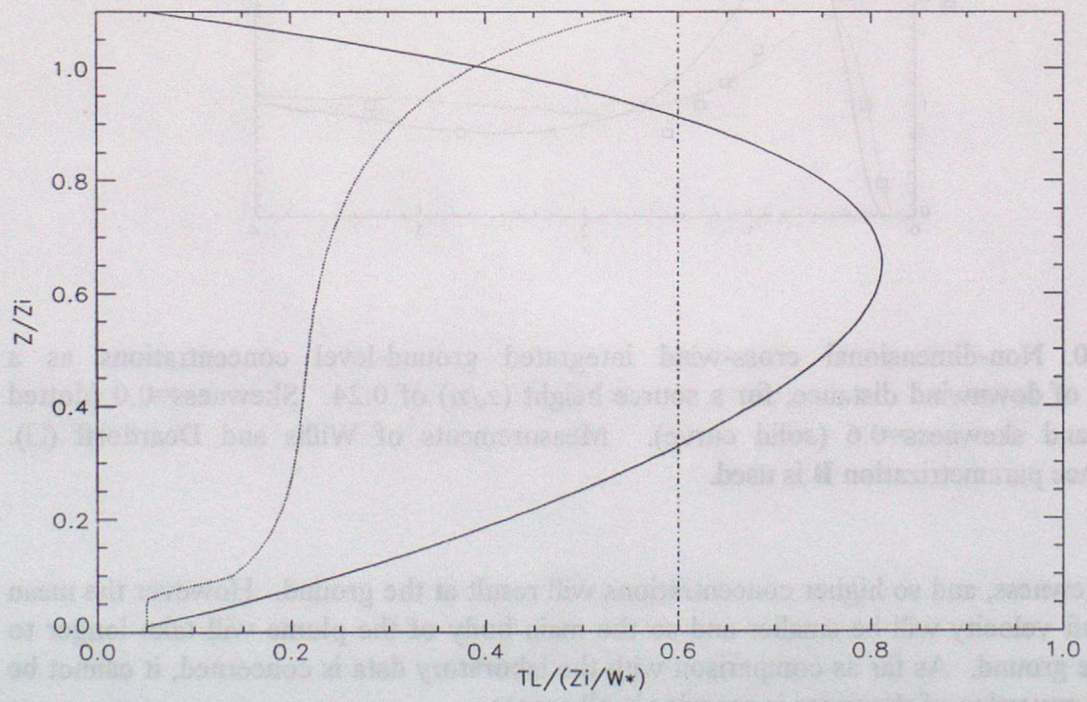

Figure 8. Profiles of Lagrangian timescale, denoted here as T_L, non-dimensionalized by (z_i/w_*) as a function of non-dimensional height z/z_i, for parametrizations **A** (dotted curve), **B** (solid curve) and **C** (dash - dot curve).

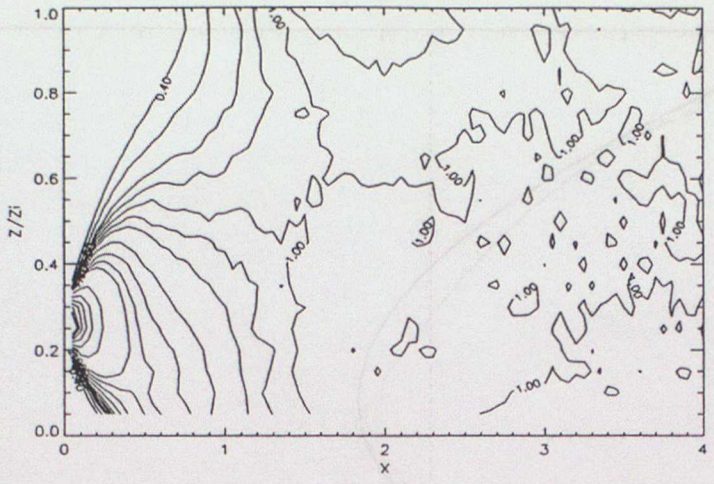

Figure 9. Contours of the non-dimensional cross-wind integrated concentrations predicted by the model using parametrization **B** (Hibberd and Sawford) and skewness=0.0 for a source height (z_s/z_i) of 0.24.

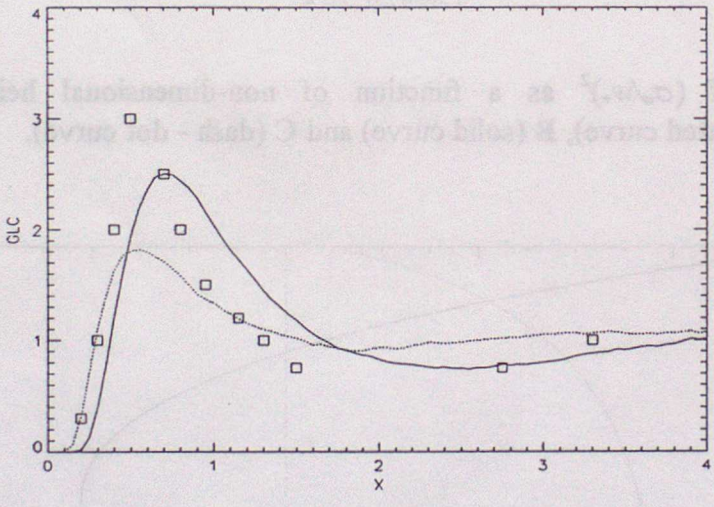

Figure 10. Non-dimensional cross-wind integrated ground-level concentrations as a function of downwind distance, for a source height (z_s/z_i) of 0.24. Skewness=0.0 (dotted curve), and skewness=0.6 (solid curve). Measurements of Willis and Deardorff (□). Turbulence parametrization **B** is used.

lower skewness, and so higher concentrations will result at the ground. However the mean downdraft velocity will be smaller and so the main body of the plume will take longer to reach the ground. As far as comparison with the laboratory data is concerned, it cannot be said that any value of skewness is superior in all aspects.

In all our numerical experiments so far we have used a profile of skewness (Sk) which is homogeneous in the vertical. Calculations of skewness from field and laboratory data indicate some vertical variation of this parameter, but the large amount of scatter has prevented any meaningful specification of this variation. However, it is instructive to

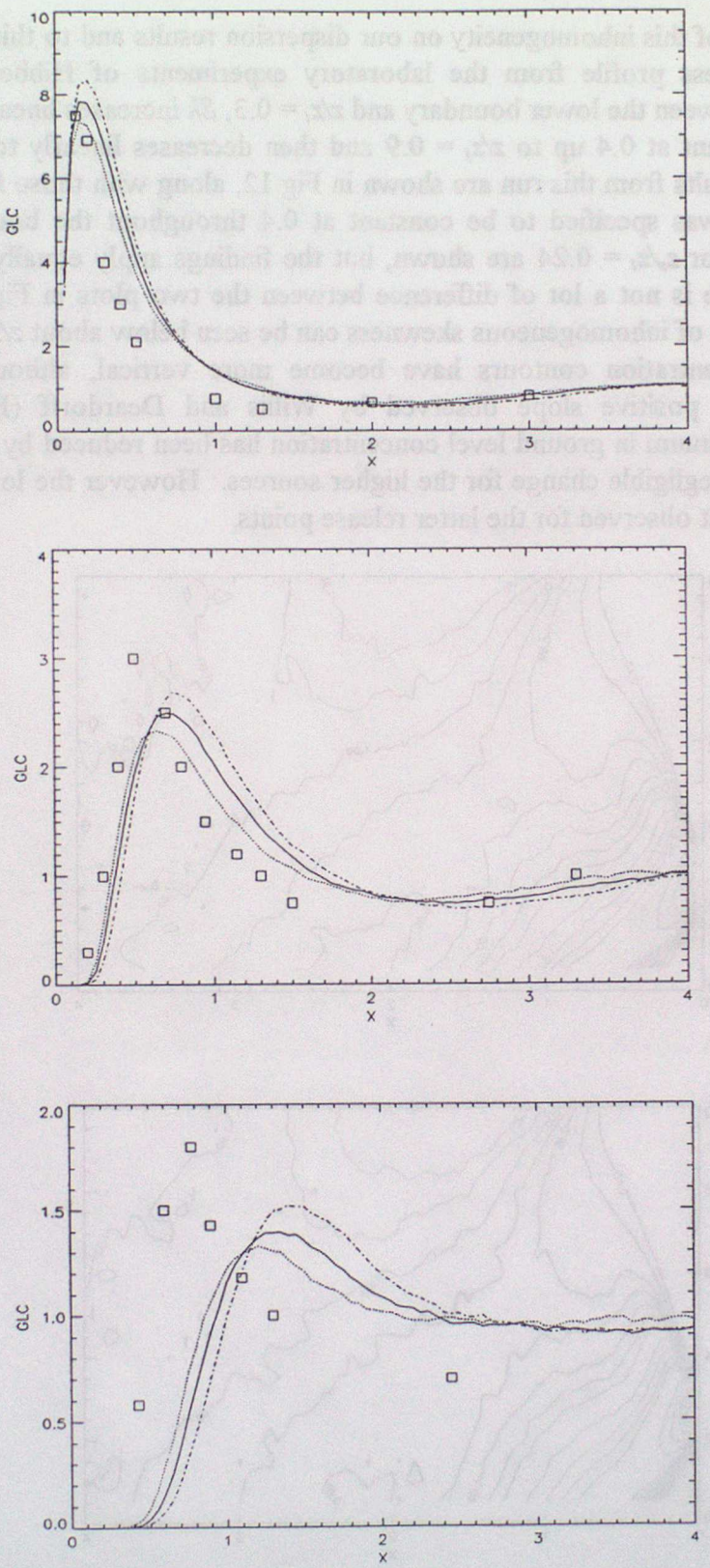

Figure 11. Non-dimensional cross-wind integrated ground-level concentrations as a function of downwind distance, for source heights (z_s/z_i): (a) 0.067, (b) 0.24, and (c) 0.49. Skewness = 0.4 (dotted curve), 0.6 (solid curve) and 0.8 (dot - dash curve). Measurements of Willis and Deardorff (□). Turbulence parametrization **B** is used.

investigate the effect of this inhomogeneity on our dispersion results and to this end we use the following skewness profile from the laboratory experiments of Hibberd (personal communication). Between the lower boundary and $z/z_i = 0.3$, Sk increases linearly from 0.0 to 0.4, remains constant at 0.4 up to $z/z_i = 0.9$ and then decreases linearly to zero at the upper boundary. Results from this run are shown in Fig.12, along with those from a run in which the skewness was specified to be constant at 0.4 throughout the boundary layer. Only concentrations for $z_s/z_i = 0.24$ are shown, but the findings apply equally to all three source heights. There is not a lot of difference between the two plots in Fig.12, but the most interesting effect of inhomogeneous skewness can be seen below about $z/z_i = 0.15$. In this region the concentration contours have become more vertical, although still not attaining the slightly positive slope observed by Willis and Deardorff (Fig.2). The magnitude of the maximum in ground level concentration has been reduced by 10% for the surface source, with negligible change for the higher sources. However the location of the maximum is nearer that observed for the latter release points.

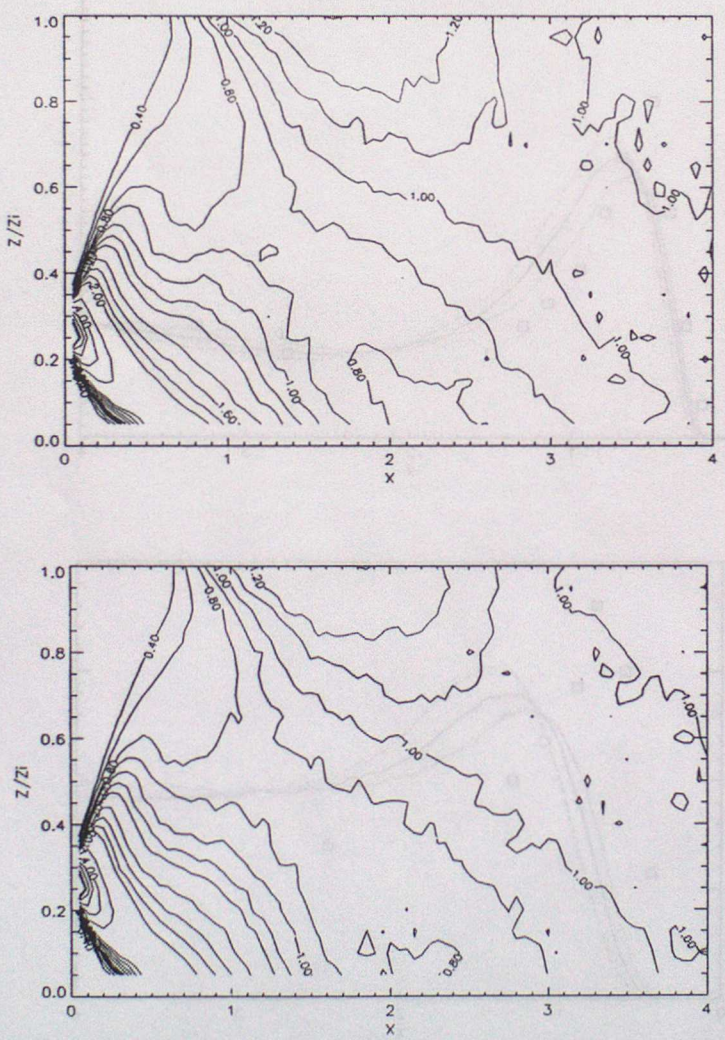

Figure 12. Contours of the non-dimensional cross-wind integrated concentrations predicted by the model using parametrization **B** (Hibberd and Sawford) for a source height (z_s/z_i) = 0.24. Skewness values used are 0.4 (upper), and an inhomogeneous profile as specified in the text (lower).

3.4.2 Universal constant C_0

There is still uncertainty over the value of C_0, although 2.0 is commonly used. Hudson and Thomson (1994) have discussed this problem and carried out random walk and large eddy simulations, concluding that C_0 should be considered a function of stability, and possibly source height. A value of 2.0 for C_0 was found to be the most suitable for convective conditions. Here we examine the effect of increasing or decreasing this value by 50%. By considering the relation $\tau_w = 2\sigma^2_w/C_o\varepsilon$, it can be seen that we are in effect decreasing by two thirds or doubling the Lagrangian timescale from its value when C_0 =2.0. Experiments are carried out with parametrization **B** and a homogeneous skewness value of 0.6.

When C_0 =3.0, the concentration distribution for all three source heights does not compare well with the Willis and Deardorff results of Fig.2; the magnitudes of the ground-level maxima are smaller than those of the C_0 = 2.0 run (Figs.4 and 6) and occur further from the source. There appears to be nothing to be achieved by pursuing values of C_0 larger than 2.0 in our model. In fact the results tend to resemble somewhat those of parametrization **A** (Figs.3 and 6). This is not too surprising as the resulting τ_w profile is similar to that of **A**.

The concentrations for each source height for the C_0 = 1.0 run are shown in Fig.13. Comparison with Figs.2 and 4 suggests that of the three C_0 values, 1.0 gives results which most closely resemble those of Willis and Deardorff. One area of improvement occurs near the ground where the contours now tend more towards the vertical, although still not as much as observed. Improvement is confirmed by Fig.14 in which ground level concentrations are compared. Not only are the magnitude and location of the glc maxima reproduced at least as well or better by C_0 = 1.0, but the region after plume lift-off where the non-dimensionalised concentrations are less than 1.0 is also simulated better. This latter feature of convective dispersion has recently been identified in the atmospheric boundary layer by Briggs (1993, 1994) in his analysis of data from the CONDORS field experiment at Boulder. For a surface source Briggs found a mean non-dimensional concentration of 0.5 at a distance of X=1.3, compared to Willis and Deardorff's values of 0.5 and 1.55 respectively. Our numerical experiments give 0.33 at X=1.65.

As mentioned above, we have in essence doubled the Lagrangian timescale τ_w for this run, leading us to conclude that the τ_w profile used in our other runs (Fig.8) is a little low, especially in the lower one third of the mixed layer. This probably explains why the homogeneous turbulence profile of Hurley and Physick (Fig.8), in which τ_w remains relatively large right down to the ground, is able to reproduce the laboratory experiments quite well. Interestingly, when this profile (parametrization **C**) is used with C_0 = 1.0 there is not a lot of difference from the results with C_0 = 2.0, although glcs after lift off are smaller, and so agree better with the data. Results for the surface source height are shown in Figs. 15 and 16. This suggests that there may be little advantage in increasing τ_w once it is sufficiently large.

3.5 Upper boundary condition

All runs discussed in this Chapter have been carried out with a skewed memory reflection condition on velocity (see section 2.2.2) at the top of the mixed layer z_i, except for the Gaussian run which employed perfect reflection. However, we have also done simulations

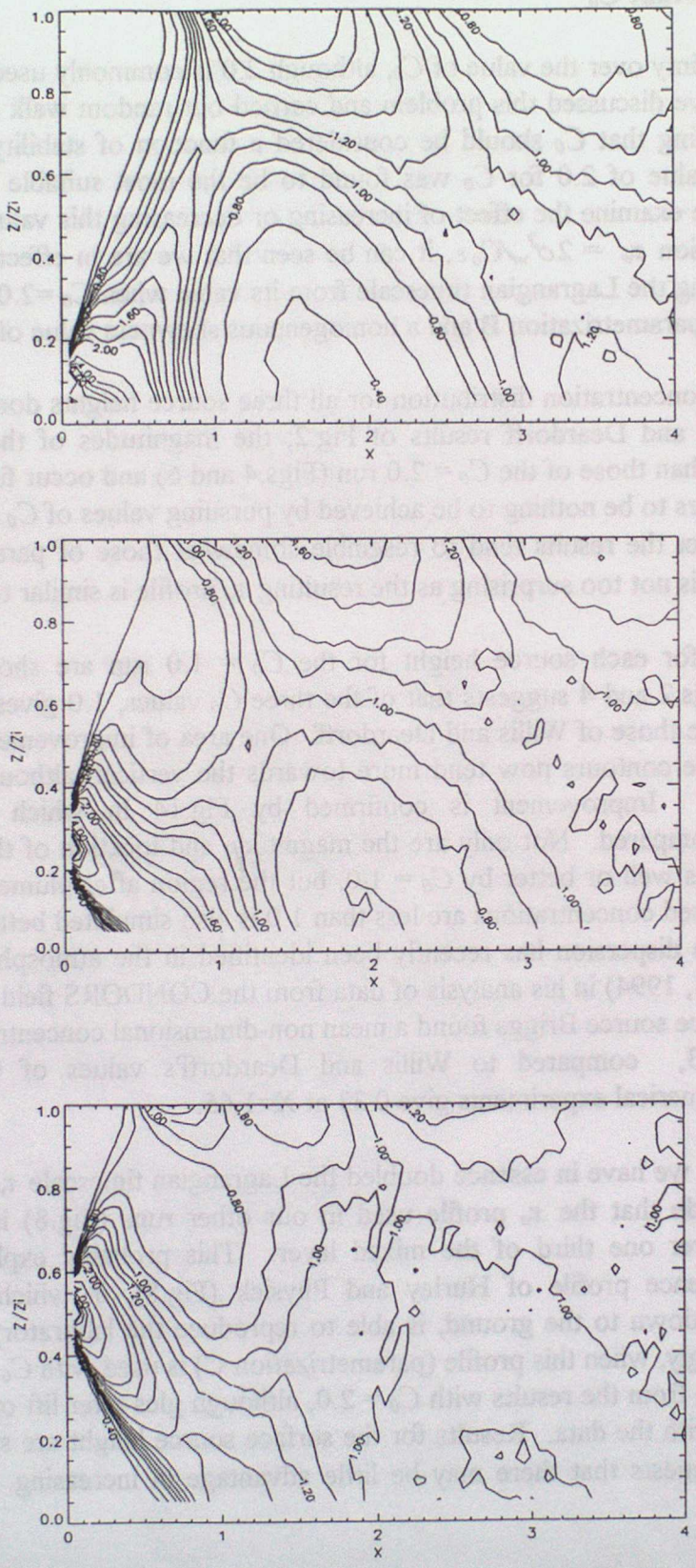

Figure 13. Contours of the non-dimensional cross-wind integrated concentrations predicted by the model using parametrization **B** (Hibberd and Sawford) and C_0 = 1.0 for the three source heights (z_s/z_i): (top) 0.067, (middle) 0.24, and (bottom) 0.49.

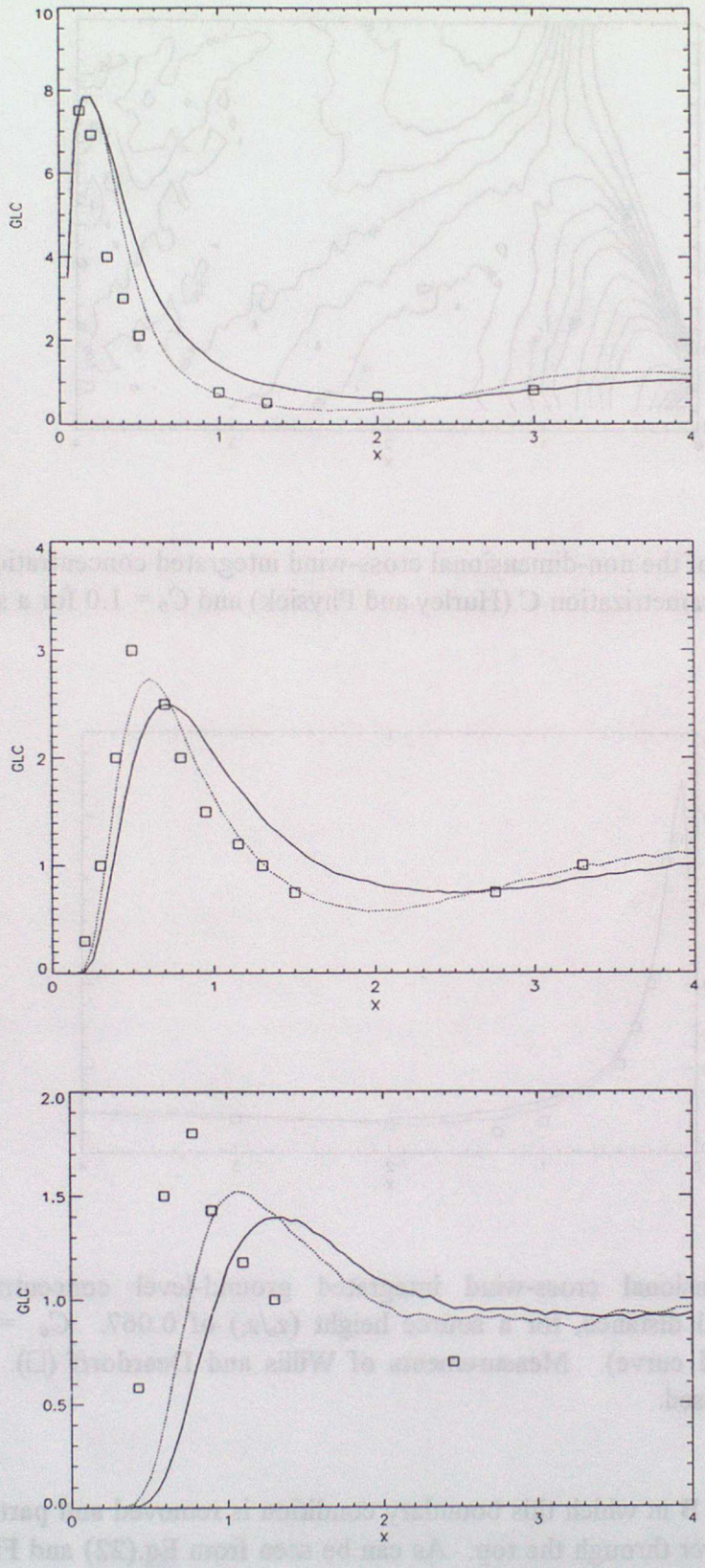

Figure 14. Non-dimensional cross-wind integrated ground-level concentrations as a function of downwind distance, for source heights (z_s/z_i): (a) 0.067, (b) 0.24, and (c) 0.49. C_0 = 1.0 (dotted curve), and 2.0 (solid curve). Measurements of Willis and Deardorff (□). Turbulence parametrization B is used.

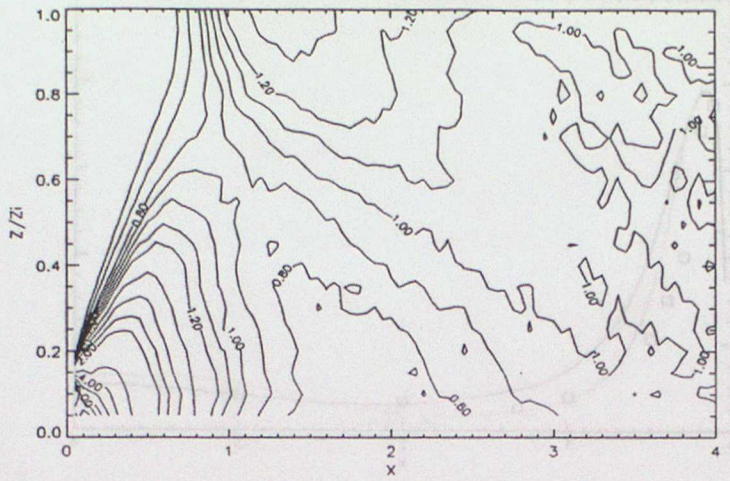

Figure 15. Contours of the non-dimensional cross-wind integrated concentrations predicted by the model using parametrization **C** (Hurley and Physick) and C_0 = 1.0 for a source height (z_s/z_i) of 0.067.

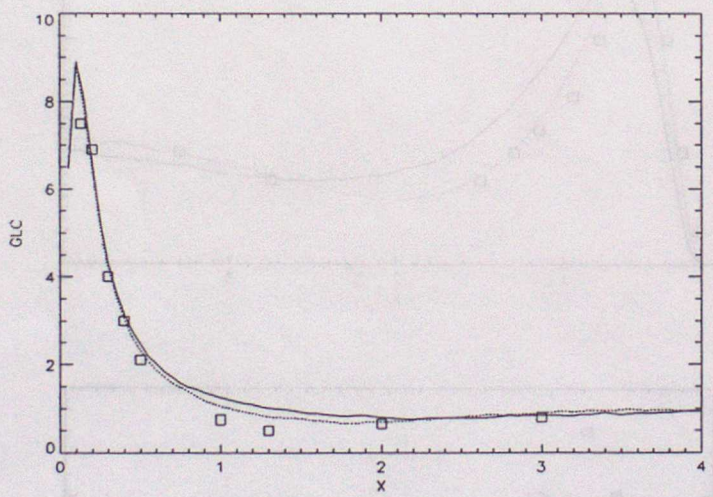

Figure 16. Non-dimensional cross-wind integrated ground-level concentrations as a function of downwind distance, for a source height (z_s/z_i) of 0.067. C_0 = 1.0 (dotted curve), and 2.0 (solid curve). Measurements of Willis and Deardorff (□). Turbulence parametrization **C** is used.

using parametrization **B** in which this boundary condition is removed and particles are free to leave the mixed layer through the top. As can be seen from Eq.(22) and Fig.7, σ_w does not go to zero at z_i, but at z=(1.0/0.9)z_i. In these runs we allow σ_w to decrease to a minimum value of .01 m s^{-1} above z_i and maintain it at this value at higher levels, on the assumption that the mixed layer is overlain by a stable layer in which turbulence is negligible.

Our main aim was to investigate the behaviour of particles near and above z_i and to see whether a well-mixed profile could be maintained. Fig.17 shows the particle distribution out to X=8 from a source at z_s/z_i =0.49, using parametrization **B** with skewness 0.6 and C_0=2.0. It is obvious that a well-mixed profile exists beyond X=4.0 and up to a height of about $1.1z_i$, that there is minimal leakage of particles to higher levels, and that the essential features of elevated source dispersion are simulated (c.f. Fig.4). Note that an *a priori* assumption of well-mixedness up to an arbitrary height of $1.5z_i$ has been assumed in Fig.17 and so the normalised concentrations should not agree with those of Fig.4 (well-mixedness assumed up to z_i). In the Fig.17 results, a value of 20 seconds was used for τ_w in the region where σ_w=.01 m s^{-1}. No difference was detected in runs in which values of 100 and 500 seconds were specified.

Simulations were also done to investigate whether particles initially above z_i could be entrained into the mixed layer, and to what extent. For a run in which particles were initially distributed uniformly between 1.0 and $1.1z_i$, it was found that by X=4.0 nearly all had been entrained into the mixed-layer, whereas for an initial spread between 1.05 and $1.15z_i$ the majority of particles remained aloft.

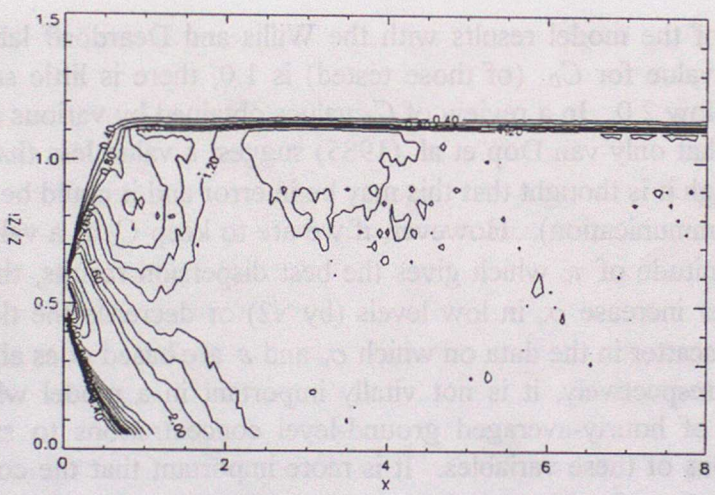

Figure 17. Contours of the non-dimensional cross-wind integrated concentrations predicted by the model using parametrization **B** (Hibberd and Sawford) for source height (z_s/z_i)= 0.49. No top boundary condition is applied (see text).

3.6 Comparison of run times

Total run time and mean timestep values for selected runs are shown in Table 1. For all runs with C_0 = 2.0, the size of the timestep is determined by $\Delta t = .05\tau_w$ for more than 96% of the time. Hence the longer run times for lower source heights when particles spend more time at levels where τ_w is smaller. For the C_0 = 1.0 runs, the timestep does not quite double because it is additionally determined in these runs for about 25% of the time by criteria (20) and (21) of section 2.3. Note that although the inhomogeneous runs with homogeneous skewness, inhomogeneous skewness and zero skewness (Gaussian) all run with the same mean timestep (6.9 seconds), the run times vary according to the amount of computations associated with each scheme. As far as σ_w is concerned, a Gaussian homogeneous profile

(not discussed in this Chapter) runs the quickest, followed by skewed homogeneous and then Gaussian inhomogeneous.

Turbulence	Param.	C_0	z_s/z_i	Mean Δt (s)	Run time (s)
skew inhomog.	B	2.0	0.49	6.9	4122
skew inhomog.	B	2.0	0.24	6.4	4500
skew inhomog.	B	2.0	0.067	5.7	5430
Gaussian inhomog.	B	2.0	0.49	6.9	3225
skew (inhom.) inhomog.	B	2.0	0.49	6.9	4441
skew homog.	C	2.0	0.49	10.0	2216
skew inhomog.	B	1.0	0.49	11.8	2496
skew homog.	C	1.0	0.49	18.3	1328
Gaussian homog.	C	1.0	0.49	18.2	1115

Table 1. Mean timestep and run time of various simulations.

3.7 Discussion

Although comparison of the model results with the Willis and Deardorff laboratory data suggests that the best value for C_0 (of those tested) is 1.0, there is little support in the literature for a value below 2.0. In a review of C_0 values obtained by various investigators, Rodean (1991) found that only van Dop et al. (1985) suggest a value less than 2.0. Their value is 1.6±0.6, although it is thought that this may be in error and it could be closer to 4.0 (Thomson, personal communication). However, if we are to keep C_0 at a value of 2.0 but also maintain that magnitude of τ_w which gives the best dispersion results, then our other alternatives are to either increase σ_w in low levels (by $\sqrt{2}$) or decrease the tke dissipation rate ε (by half). While scatter in the data on which σ_w and ε are based does allow for some increase and decrease respectively, it is not vitally important in a model which is based around the prediction of hourly-averaged ground-level concentrations to specify highly accurate parametrizations of these variables. It is more important that the combination of σ_w, ε and C_0 gives a value of τ_w that produces realistic dispersion results. It is therefore recommended that a value of 1.0 be used for C_0 in this model with the inhomogeneous turbulence parametrization **B** (Hibberd and Sawford). Although an inhomogeneous profile of skewness does give slightly better results than a constant skewness value, in view of the uncertainty of the exact nature of this profile and the fact that it produces a longer running time, it is recommended that a homogeneous skewness value of 0.6 be used.

It should be noted that the skewed homogeneous parametrization **C** gives very good results and a considerably faster running time. Results from runs in which the timestep has been increased to $0.15\tau_w$ are barely different from the $0.05\tau_w$ results and of course run three times faster.

While a Gaussian homogeneous turbulence profile does not reproduce near-source dispersion well, it is able to maintain a well-mixed profile and could be used further from the source where its relatively fast computation time (see Table 1) would be an advantage.

4. BOUNDARY-LAYER TURBULENCE PROFILES USED IN NAME

This Chapter presents details of the turbulence parametrizations (velocity variance σ^2, Lagrangian timescale τ or turbulence dissipation rate ε) used in the near-source version of NAME. These will differ depending on the stability of the atmospheric boundary layer and for the horizontal and vertical turbulent components. The current version of the Unified Model (UM) is hydrostatic with a flux-gradient type turbulence closure, so that the direct route of utilizing diagnosed turbulent kinetic energy is denied. The values must be determined either from empirical fits to observational data, or parametrized from the information stored in the UM using, eg. *Ri*-based formulae. The former option has been chosen for the NAME parametrization. For the unstable boundary layer, we employ the turbulence profiles of Hibberd and Sawford (1994) and Hurley and Physick (1993)---see evaluation in Chapter 3---with a mechanical component or neutral limit from Brost et al 1982. It is convenient to express the formulae in z-coordinates (height above the ground) rather than the model η-coordinate system.

4.1 Stable Boundary Layer

At night the atmosphere becomes stably stratified due to radiative cooling from the surface beneath, and turbulence tends to be suppressed. Typically it takes the form of slow oscillations of wind direction with intermittent bursts of mechanically driven turbulence, depending on the wind strength. The formulae for stable conditions are adopted from Hanna's (1982) review:

$$\sigma_u = \sigma_v = 2.0u_*\left(1 - z/z_i\right)$$
$$\sigma_w = 1.3u_*(1 - z/z_i)$$
$$\frac{d\sigma_w}{dz} = -\frac{1.3u_*}{z_i}$$

and the timescales

$$\tau_u = \tau_v = 0.07\frac{z_i}{\sigma_v}\left(\frac{z}{z_i}\right)^{1/2}$$
$$\tau_w = 0.10\frac{z_i}{\sigma_w}\left(\frac{z}{z_i}\right)^{0.8}$$

4.2 Unstable and Neutral Boundary Layers

Unstable or convective conditions occur where the air is buoyant due to heating from the surface. The boundary layer is deepened steadily by the action of thermals on the capping inversion, and reaches a maximum (which may be a km or two) by late afternoon. Turbulent mixing is due to both buoyant overturning and mechanical turbulence, which decay in the mixed layer after sunset. At these times of transition between convective and stable conditions, or when the weather conditions are generally overcast and windy, the heat

flux to and from the surface is near zero, and the atmosphere is described as neutral. The profiles used are as follows.

Near - source: Skewed inhomogeneous turbulence

$$\frac{\sigma_w}{w_*} = \left[1.2\left(\frac{z}{z_i}\right)^{2/3}\left(1 - 0.9\frac{z}{z_i}\right)\right]^{\frac{1}{2}}$$ (Hibberd and Sawford, 1994)

can apply only towards the convective limit; accordingly a mechanical term derived from the profiles in Brost et al (1982) has been incorporated into the formula using a root sum of squares to give

$$\sigma_w = \left[1.2w_*^2\left(1 - 0.9\frac{z}{z_i}\right)\left(\frac{z}{z_i}\right)^{\frac{2}{3}} + \left(1.8 - 1.4\frac{z}{z_i}\right)u_*^2\right]^{\frac{1}{2}}$$

so that

$$\frac{d\sigma_w}{dz} = \frac{1}{\sigma_w z_i}\left\{ w_*^2\left(\frac{z}{z_i}\right)^{-\frac{1}{3}}\left(0.4 - 0.9\frac{z}{z_i}\right) - 0.7u_*^2\right\}$$

These formulae can also, of course, be applied in the neutral limit. A.R.Brown (private communication) has found from LES integrations that although formulae which exclude the mechanical contribution are inadequate, the inclusion of the full neutral component can give results which are a little excessive. A cube root sum of cubes may be preferable---see for example Moeng and Sullivan (1994). The formulae will be reviewed when further experience has been gained. Similarly,

$$\sigma_u = \sigma_v = \left[0.4w_*^2 + (5 - 4z/z_i)u_*^2\right]^{\frac{1}{2}}$$

but for the surface layer, for $\eta > 0.996$, after Hanna (1982),

$$\sigma_u = \sigma_v = u_*(1.2 + 0.5z_i/|L|)^{\frac{1}{3}}.$$

It will be noted these formulae give a profile for σ up to about $z/z_i = 1.3$. In addition,

$$Sk = 0.6 \qquad C_0 = 1.0.$$

The formula for the dissipation rate of TKE is a combination of convective and neutral terms from Luhar and Britter (1989) and a fit to the profile in Grant (1992), respectively:

$$\varepsilon = \left(1.5 - 1.2\left(\frac{z}{z_i}\right)^{\frac{1}{3}}\right)\frac{w_*^3}{z_i} + \frac{u_*^3(1-0.8z/z_i)}{kz}$$

subject to a minimum of 10^{-6}, so that

$$\tau_{u,v,w} = 2\sigma_{u,v,w}^2 / C_0\varepsilon.$$

Medium-range: Gaussian homogeneous turbulence

$$\sigma_u = \sigma_v = \left[0.4w_*^2 + 3u_*^2\right]^{\frac{1}{2}}$$

$$\sigma_w = \left[0.4w_*^2 + 1.1u_*^2\right]^{\frac{1}{2}}$$

$\varepsilon = 0.6w_*^3 / z_i + 1.2u_*^3 / kz_i$ used to compute τ, as above,

$Sk = 0.0$ $C_0 = 1.0$

In unstable conditions, the mode of operation envisaged is that a switch be used to effect a transition from a skewed inhomogeneous turbulence parametrization close to the source to Gaussian homogeneous in the middle field to the existing NAME parametrization (Maryon and Buckland, 1994) of random reassignment in the vertical (assuming a well-mixed layer) in the far field. In this way an optimum timestep can be used at the various stages of a simulation while still reproducing the essential features of convective dispersion.

4.3 Boundary Conditions

The specification for the NAME model follows. Two problems arise in the vicinity of the capping inversion: the vertical gradients $\partial\sigma_w / \partial z$ due to the particle motion during a timestep---for the inhomogeneous profiles this is catered for in the model formulation---and the changes in time $\partial\sigma_w / \partial t$ due to the rediagnosis of boundary layer depth at intervals, which can result in a particle 'crossing' the inversion. This is not allowed for in the random walk model. Accordingly a rather complex set of boundary conditions have to be applied, which is summarised in Table 2.

Vertical

Unstable/neutral boundary layer---inhomogeneous: Above the inversion use a minimum of 0.01m/sec for σ_w and zero gradients---the inhomogeneous formulae of section 4.2 give usable values up to about 1.3 times the boundary layer depth. Where the skewed option applies the variable α (section 2.1.2) is not standardised, and must be rescaled whenever a particle crosses the inversion.

Unstable/neutral boundary layer---homogeneous: The step change in σ_w would have a serious impact on the distribution of particles crossing the inversion, so that a reflection as

described in section 2.2 will be used initially. There will be no serious degrading of the integration , as the conditioned particle motion will only be operating for a short space of time. The minimum of 0.01m/sec is used above the inversion. Particles crossing the inversion due to changes in the diagnosed inversion height must be re-initialised. Improved top boundary conditions will be developed in due course.

Stable boundary layer: Use a minimum of 0.01m/sec for σ_w; thus a test will be necessary below the inversion. Zero gradient applies above the inversion.

Changes in profile	UNSTABLE						STABLE
of	Homogeneous			Inhomogeneous			
	Neutral	Gaussian	Skewed	Skewed	Gaussian	Neutral	
$\partial\sigma/\partial z \Rightarrow$							
	jump at z_i	jump at z_i	jump at z_i	continuous	continuous	continuous	continuous
	reflect	reflect	reflect	no action	no action	no action	no action
$\partial\sigma/\partial t \Rightarrow$							
	$\alpha = \dot{\eta}'/\sigma_\eta$	$\alpha = \dot{\eta}'/\sigma_\eta$	$\alpha = \dot{\eta}'$	$\alpha = \dot{\eta}'$	$\alpha = \dot{\eta}'/\sigma_\eta$	$\alpha = \dot{\eta}'/\sigma_\eta$	$\alpha = \dot{\eta}'/\sigma_\eta$
	initialise	initialise	initialise	rescale	no action	no action	no action

Table 2. Boundary conditions for the different categories of stability and homogeneity.

Horizontal

Unstable and neutral boundary layers: use $\sigma_u = \sigma_v = 0.05\,\text{m/sec}$ above the inversion pending further investigation. It is considered safest to re-initialise particles crossing the capping inversion. The model does not, at present, handle $\partial\sigma_{u,v}/\partial z$, or even scale u', v' in terms of α : these matters will be addressed at a later date.

Stable boundary layer: Use a minimum of 0.05m/sec: again a test will be necessary below the inversion.

Timescales

For lack of information the following values will be used above the boundary layer:
$\tau_u = \tau_v = \tau_w = 300\,\text{sec}$
in order to provide a reasonable timestep.

Future work will focus on an improved entrainment parametrization and the efficacy of the CBL formulae combining u_* and w_*.

4.4 A Note on Computation

The truncation effects in long integrations are surprising. Minute effects due to slight rearrangements of the code can lead to a prolonged, slow change in particle level, vertical velocity impulse and computed timestep. Ultimately an additional timestep (or part thereof)

is needed in one arrangement to reach the end of an integration period: this alters the incidence of the random numbers generated for the remainder of the integration, and from hereon changes increase steadily. For skew runs these changes may be accelerated close to the surface, where the solution of equation (20) can be very sensitive to precision.

Thus for two 2000 particle runs extending over 8 consecutive periods of 600 secs, featuring a slight difference in the arrangement of the algebra computing $\partial\sigma_w / \partial z$, no significant change occurred before particle number 1410 at the end of period 7. At this point an extra timestep was needed in one of the runs to reach the 600secs termination. Beyond this point the differences mounted steadily due to the changed allocation of the random numbers. The differences in the length of the timestep increased monotonically through period 7, arguing a systematic feedback.

Truncation effects due to different computational approaches can hence lead to different *realizations* , although there may be little justification for assuming that one is more 'valid' than another.

ACKNOWLEDGEMENT: Our thanks to D J Thomson , Meteorological Office, for his advice, and for comments on this paper.

REFERENCES

Adrian, R.J., Ferreira, R.T.D.S. and Boberg, T. (1986) Turbulent thermal convection in wide horizontal fluid layers. *Experiments in Fluids,* **4,** 121-141.

Briggs, G.A. (1993a) Final results of the CONDORS convective diffusion experiment. *Boundary-Layer Met.*, **62**, 315-328.

Briggs, G.A. (1993b) Plume dispersion in the convective boundary layer. Part II: analyses of CONDORS field experiment data. *J. Appl. Meteor.*, **32**, 1388-1425.

Brost, R.A., Wyngaard, J.C. and Lenschow, D.H. (1982) Marine stratocumulus layers. Part II: Turbulence budgets. *J. Atmos. Sc.* **39,** 818-836.

Caughey, S.J. and Palmer, S.G. (1979) Some aspects of turbulence structure through the depth of the convective boundary layer. *Q. Jl. R. Met. Soc.*, **105**, 811-827.

Deardorff, J.W. and Willis, G.E. (1985) Further results from a laboratory model of the convective planetary boundary layer. *Boundary-layer Met.*, **32**, 205-236.

de Baas, A.F., van Dop, H. and Nieuwstadt, F.T.M. (1986) An application of the Langevin equation for inhomogeneous conditions to dispersion in a convective boundary layer. *Q. Jl. R. Met. Soc.*, **112**, 165-180.

Grant, A.L.M. (1992) The structure of turbulence in the near-neutral atmospheric boundary layer. *J. Atmos. Sc.* **49**, 226-239.

Hanna, S.R. (1982) Applications in air pollution modeling. In: Atmospheric Turbulence and Air Pollution Modeling. Ed.F.T.M. Nieuwstadt and H. van Dop, D Reidel Publishing Company, Dordrecht, Holland.

Hibberd, M.F. and Sawford, B.L. (1994) A saline laboratory model of the planetary convective boundary layer. *Boundary-Layer Met.*, **69**, 229-250.

Hudson, B. and Thomson, D.J. (1994) Dispersion in convective and neutral boundary layers using a random walk model. Met O (APR) Turbulence and Diffusion Note No. 210.

Hurley, P.J. and Physick, W.L.(1993) A skewed homogeneous Lagrangian particle model for convective conditions. *Atmospheric Environment*, **27A, No. 4**, 619-624.

Kumar, R. and Adrian, R.J. (1986) Higher order moments in the entrainment zone of turbulent penetrative thermal convection. *Trans, ASME,J Heat Transfer,* **108**, 323-329.

Lamb, R.G. (1978) Numerical simulation of dispersion from an elevated point source in the convective boundary layer. *Atmospheric Environment,* **12,** 1297-1304.

Lemone, M.A., (1990) Some observations of vertical velocity skewness in the convective planetary boundary layer. *J. Atmos. Sci.*, **47**, 1163-1169.

Luhar, A.K. and Britter, R.E (1989) A random walk model for dispersion in inhomogeneous turbulence in a convective boundary layer. *Atmospheric Environment*, **23**, 1911-1924.

Maryon, R.A. and Buckland, A.T. (1994) Diffusion in a Lagrangian multiple particle model: a sensitivity study. *Atmos. Environ.*, **28**, 2019-2038.

Moeng, C-H. and Sullivan, P.P. (1994) A comparison of shear- and buoyancy-driven planetary boundary layer flows. *J. Atmos. Sc.* **51,** 999-1022.

Nieuwstadt, F.T.M., Mason, P.J., Moeng, C.H., and Schumann, U. (1992) Large-eddy simulation of the convective boundary layer: A Comparison of Four Computer Codes *Turbulent Shear Flows,* **8**, Springer, pp 343-367.

Physick, W.L. and Hurley, P.J. (1995) A fast Lagrangian particle model for use with three-dimensional mesoscale models. *20th International Technical Meeting on Air Pollution Modelling and its Application, X,* Ed. E. Gryning and M. Millan, Plenum Press, New York.

Rodean, H.C. (1991) The universal constant for the Lagrangian structure function. *Phys. Fluids A*, **3**, 1479-1480.

Sawford, B.L. and Guest, F.M. (1987) Lagrangian stochastic analysis of flux gradient relationships in the convective boundary layer. *J Atmos Sci,* **44,** 1152-1165.

Thomson, D.J. (1984) Random walk modelling of diffusion in inhomogeneous turbulence. *Q. Jl. R.. Met. Soc.,* **110**, *1107-1120.*

Thomson, D.J. (1987) Criteria for the selection of stochastic models of particle trajectories in turbulent flows. *J. Fluid Mech.*, **180,** 529-556.

Thomson, D.J. and Montgomery, M.R. (1994) Reflection boundary conditions for random walk models of dispersion in non-Gaussian turbulence. *Atmospheric Environment*, **28,** 1981-1987.

van Dop, H., Nieuwstadt, F.T.M. and Hunt, J.C.R. (1985) Random walk models for particle displacements in inhomogeneous unsteady turbulent flows. *Phys. Fluids*, **28,** 1639-1653.

Willis, G.E. and Deardorff, J.W. (1974) A laboratory model of the unstable planetary boundary layer. *J Atmos Sci.*, **31,** 1297-1307.

Willis, G.E. and Deardorff, J.W. (1976) A laboratory model of diffusion into the convective planetary boundary layer. *Q. Jl R.Met. Soc.*, **102,** 427-445.

Willis, G.E. and Deardorff, J.W. (1978) A laboratory study of dispersion from an elevated source within a modeled convective planetary boundary layer. *Atmospheric Environment*, **12,** 1305-1311.

Willis, G.E. and Deardorff, J.W. (1981) A laboratory study of dispersion from a source in the middle of the convective mixed layer. *Atmospheric Environment*, **15,** 109-117.

Wilson, J.D., Legg, B.J. and Thomson, D.J. (1983) Calculation of particle trajectories in the presence of a gradient in turbulent-velocity variance. *Boundary-Layer Met.*, **27,** 163-169.

Wyngaard, J.C. (1988) Structure of the PBL. In: Air Pollution Modeling, Ed, A Venkatram and J C Wyngaard, American Meteorological Society, Boston, USA, 390pp.

Young, G.S. (1988) Turbulence structure of the convective boundary layer. Part I: Variability of normalized turbulence statistics. *J. Atmos. Sci.*, **45**, 719-726.